Journal of Nanobiotechnology

RESEARCH Open Access

A novel HER2 targeting nanoagent self-assembled from affibody-epothilone B conjugate for cancer therapy

Xuelin Xia[1], Xiaoyuan Yang[1], Wenhui Gao[1], Wei Huang[1], Xiaoxia Xia[2*] and Deyue Yan[1*]

Abstract
Epothilone B (Epo B), a promising antitumor compound effective against various types of cancer cells in vitro. However, its poor selectivity for tumor cells and inadequate therapeutic windows significantly limit its potential clinical application. Affibody is a class of non-immunoglobulin affinity proteins with precise targeting capability to overexpressed molecular receptors on cancer cells, has been intensively investigated due to its exceptional affinity properties. In this study, we present a targeted nanoagent self-assembled from the precursor of an affibody conjugated with Epo B via a linker containing the thioketal (tk) group that is sensitive to reactive oxygen species (ROS). The core-shell structure of the $Z_{HER2:342}$-Epo B Affibody-Drug Conjugate Nanoagent (Z-E ADCN), with the cytotoxin Epo B encapsulated within the $Z_{HER2:342}$ affibody corona, leads to significantly reduced side effects on normal organs. Moreover, the abundant presence of $Z_{HER2:342}$ on the surface effectively enhances the targeting capacity and tumor accumulation of the drug. Z-E ADCN can be internalized by cancer cells via HER2 receptor-mediated endocytosis followed by Epo B release in response to high levels of ROS, resulting in excellent anticancer efficacy in HER2-positive tumor models.

Keywords Epothilone B, Affibody, Self-assemble, Drug delivery, Targeted cancer therapy

Introduction

Epothilones are a class of 16-membered macrolides derived from the myxobacterium *Sorangium cellulosum* [1]. These natural epothilones compounds exhibit potent activity against various types of cancer cells in sub-nanomolar range by stabilizing microtubules and inducing apoptosis [2, 3]. In comparison to other epothilones, epothilones B (EpoB) shows particularly stronger anticancer activity, which has attracted a lot of research interest ever since discovery [4–6]. Up to now, a semi-synthetic analog of EpoB, named Ixabepilone (BMS-247550), has been approved by the FDA for the treatment of metastatic or locally advanced breast cancer that does not respond to anthracyclines, taxane derivatives and capecitabine [7, 8]. However, other derivatives such as Novartis' methylthio Epo B (ABJ879) and Bristol-Myers Squibb's aminomethyl Epo B (BMS-310705) have failed in clinical trial stage, which probably due to the poor bio-availability and severe side effects [9, 10]. Therefore, appropriate improvements are still necessary for the clinical application of Epo B in future.

*Correspondence:
Xiaoxia Xia
xiaoxiaxia@sjtu.edu.cn
Deyue Yan
dyyan@sjtu.edu.cn
[1]School of Chemistry and Chemical Engineering, Frontiers Science Center for Transformative Molecules, Shanghai Jiao Tong University, Shanghai 200240, People's Republic of China
[2]State Key Laboratory of Microbial Metabolism, School of Life Sciences and Biotechnology, Shanghai Jiao Tong University, Shanghai 200240, People's Republic of China

In recent decades, a variety of nanovehicles (e.g., polymers [11–13], liposomes [14, 15], and vesicles [16, 17]) have been investigated as delivery carriers to enhance the bioavailability and reduce the systemic toxicity of anticancer drugs. However, many of these carriers still encounter challenges such as lack of targeting ability, complex synthesis processes, and potential immunogenicity during organism metabolism. To address these limitations, numerous targeting biological materials (e.g., peptides [18, 19], carbohydrates [20–22], and antibodies [23, 24]) have been further developed for combination with anticancer molecules to form tumor-targeted conjugates for cancer therapy. In terms of Epo B, our group has engineered an $\alpha_v\beta_3$ integrin targeted nanoagent self-assembled from the RGD peptide-EpoB conjugate, and more recently, Lou and co-workers have developed multiple rhamnose-binding lectin (RBL) targeted nanomicelles that self-assemble from the Rhamnose-EpoB conjugate [25, 26]. All of these studies have demonstrated enhanced therapeutic windows and significant reductions in the adverse effects of Epo B. However, therapeutic efficacy of these conjugates remains suboptimal, most likely due to the limited affinity of the carrier material for their targets.

Affibody, a small (6–7 kDa) affinity protein composed of 58 amino acids arranged in a three-helix bundle, has gained significant attention for its exceptional binding affinity to several target proteins [27–29]. Benefiting from its unique structure, affibody molecules exhibits numerous potential benefits, including rapid tissue penetration owing to their diminutive size, picomolar affinities along with high selectivity, and facile production through microbial fermentation [30, 31]. Take these advantages, we have successfully developed a series of affibody-MMAE conjugates in our previous research. The resulting conjugates can self-assemble into affibody-drug conjugate nanoagents that have been demonstrated with enhanced biosafety and extraordinary antitumor activity, leading to relative tumor proliferation inhibition ratios over 99% in relevant tumor models [32, 33]. Therefore, employing affibody as a carrier of Epo B might be a meaningful attempt.

Expanding on this concept, here we prepared a nanoagent self-assembled from affibody-Epo B conjugate for targeted cancer therapy (Scheme 1). First, a HER2 (human epidermal growth factor receptor 2) targeted affibody molecule $Z_{HER2:342}$-Cys was designed and then produced using the *E. coli* expression system. Subsequently, the $Z_{HER2:342}$-Cys was conjugated with Epo B through a linker containing maleimide group and reactive oxygen species (ROS)-responsive thioketal (tk) group. Finally, the obtained conjugate was self-assembled into $Z_{HER2:342}$-Epo B Affibody Drug Conjugate Nanoagent (Z-E ADCN) in water ascribing to its inherent amphiphilic structure (Scheme 1A). The core shell structure of Z-E ADCN with Epo B encapsulated inside the $Z_{HER2:342}$ corona significantly reduces drug exposure in the bloodstream, resulting in reduced side effects to normal organs. Meanwhile, benefiting from the large amount of $Z_{HER2:342}$ on the surface, Z-E ADCN can effectively target to the tumor site and then be internalized by cancer cells through HER2-specific receptor mediated endocytosis (Scheme 1B). Owing to the extracellular oxidative matrix and high levels of intracellular ROS [34–36], free Epo B can be effectively released in tumor tissues by the degradation of tk group, thereby inducing effective apoptosis of cancer cells.

Materials and methods

Materials

Epothilones B (Epo B) was supplied by Zhejiang Hisun Pharmaceutical Co., Ltd. Escherichia coli DH5α and BL21 Star (DE3) were acquired from Invitrogen (Life Technologies Corp., Carlsbad, CA). Enterokinase was obtained from Yeasen Biotech Co., Ltd. (Shanghai, China). The cell counting kit-8 (CCK-8) assay and Annexin V-FITC/PI apoptosis detection kit were also purchased from Invitrogen. Tris(2-carboxyethyl) phosphine (TCEP) was bought from Adamas, while all other reagents were sourced domestically. Standard protocols were followed for all molecular biology procedures.

Preparation of $Z_{HER2:342}$-Cys

The plasmid encoding the recombinant $Z_{HER2:342}$ affibody was successfully introduced into competent E. coli BL21 Star (DE3) cells. The cells were extended cultured and then induced with 1 mM isopropyl-β-D-thiogalactopyranoside (IPTG) at a temperature of 16°C overnight. After that, the cell were collected and crushed using ultrasonic. The $Z_{HER2:342}$ affibody was finally obtained via the purification of Ni-nitrilotriacetyl agarose column, followed by dialysis against water and lyophilization for storage. Following this, a solution of $Z_{HER2:342}$-Cys-EK-His and enterokinase in reaction buffer was stirred at 25°C overnight. The resulting reaction solution was dialyzed against water to eliminate the His-tag residue. Finally, the $Z_{HER2:342}$-Cys was collected and lyophilized for storage. All of the obtained affibody were confirmed using Matrix-Assisted Laser Desorption/Ionization Time of Flight Mass Spectrometry (MALDI-TOF-MS).

Synthesis of epo B-tk-MAL

The Epo B-tk-MAL compound was synthesized according to our previous methodology [26]. Firstly, the mixture of 3,3′-(Propane-2,2-diylbis(sulfanediyl)) Dipropionic Acid (252.05 mg, 1 mmol), EDCI (287.55 mg, 1.5 mmol), DMAP (12.2 mg, 0.1 mmol) and anhydrous TEA (0.28

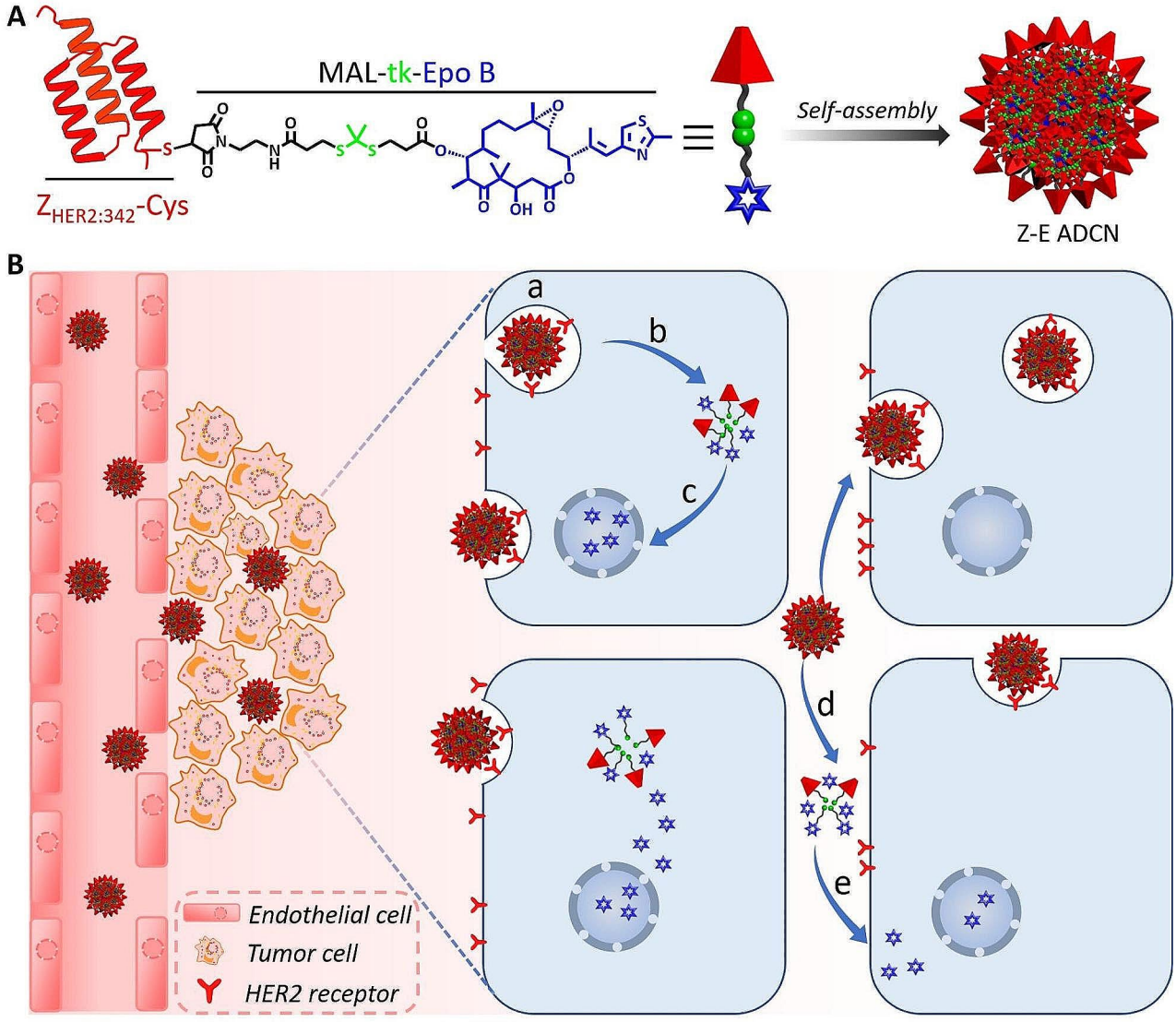

Scheme 1 Illustration of $Z_{HER2:342}$-Epo B Affibody Drug Conjugate Nanoparticles (Z-E ADCN) for targeted drug delivery. (**A**) Depiction of the chemical structure and self-assembly process of $Z_{HER2:342}$-Epo B to form Z-E ADCN. (**B**) Visualization of the active tumor-targeting delivery mechanism of Z-E ADCN, including (a) HER2 receptor mediated transcytosis, (b) Disassembly within cells due to intracellular high levels of ROS, (c) Intracellular entry and induction of apoptosis by Epothilone B, (d) Extracellular degradation leading to release of Epothilone B due to oxidative extracellular matrix, (e) Diffusion into surrounding cells and induction of apoptosis by the released Epothilone B

mL, 2 mmol) in anhydrous CH_2Cl_2 was stirred at room temperature for 1 h. Then Epo B (507.27 mg, 1 mmol) was added and the mixture was stirred for 24 h. The solution was then washed with deionized water and the organic phase was collected and purified by column chromatography to obtain Epo B-tk-COOH as a white powder.

After that, Epo B-tk-COOH (74.13 mg, 0.1 mmol), HATU (57.04 mg, 0.15 mmol) and DIPEA (21 μL, 0.15 mmol) were dissolved in anhydrous CH_2Cl_2 and stirred at room temperature for 0.5 h. Then N-(2-aminoethyl) maleimide trifluoroacetate salt (38.12 mg, 0.15 mmol), and DIPEA (21 μL, 0.15 mmol) were added to the solution and stirred for 6 h. The solution was then filtered and washed with deionized water before the organic phase was collected and purified by column chromatography to obtain Epo B-tk-MAL as a white powder.

Preparation of $Z_{HER2:342}$-Epo B ADCN

Briefly, 10 mg of $Z_{HER2:342}$-Cys was dissolved in 5 mL of deionized water with the addition of 0.1 μM TCEP, and 1.22 mg of Epo B-tk-MAL was dissolved in 150 μL of DMSO. The drug-containing DMSO was then added to the $Z_{HER2:342}$-Cys solution under magnetic stirring for 10 h, the resulting mixture underwent purification through dialysis against deionized water to remove

uncombined raw material. Finally, a stable bluish $Z_{HER2:342}$-Epo B ADCN solution was obtained.

Preparation of Cy5.5 labeled conjugates

5 μM of Sulfo-Cyanine5.5 NHS ester and 1 μM of $Z_{HER2:342}$-Cys were mixed in PBS at room temperature and stirring for 4 h. The unreacted Sulfo-Cyanine5.5 NHS ester was then removed using a PD MiniTrap G-25 column to obtain the solution of Cy5.5-labeled $Z_{HER2:342}$-Cys. The amount of Cy5.5 in $Z_{HER2:342}$-Cys was determined using spectrophotometer. Subsequently, Cy5.5-labeled Z-E ADCN was synthesized using the same method as described above.

Biospecific affinity analysis

The interactions between the extracellular domain (ECD) of HER2 and affibody molecules were assessed using biosensor analysis on a Biacore 8 K system. HER2-ECD was immobilized on a CM5 chip at an approximate level of 1000 resonance units (RU). The affinity constants were determined by injecting a range of diluted concentrations as needed.

Cell culture

SKOV-3 cells (a human ovarian cancer cell line) were cultured with McCoy's 5 A medium, MCF-7 cells (a human breast adenocarcinoma cell line) and L929 cells (a mouse fibroblast cell line) were cultured with complete DMEM medium, both medium containing 10% FBS and 1% antibiotic. All these cells were purchased from the cell bank of Chinese Academy of Sciences.

In vitro ROS Responsiveness of Z-E ADCN

5×10^5 SKOV-3 cells were seeded in each well and then Z-E ADCN was added at a concentration of 10 μM for 12 h at 37 °C. Subsequently, the medium was aspirated and 1 mL of methanol and cold PBS mixture (v/v, 1:1) was added to each well, the cells were collected and disrupted via sonication. The resulting supernatant was obtained through centrifugation and then lyophilized. The resultant sample was redissolved in acetonitrile and subjected to analysis by LC-MS.

Cellular uptake

For the flow cytometry (FCM) analysis, SKOV-3 cells were seeded at a density of 5×10^5 cells per well and cultured overnight. Subsequently, the diluted Cy5.5-labeled Z-E ADCN solution (10 μM) was added to different wells, followed by incubation for specific time intervals at 37 °C. The collected cells were then analyzed using FCM. For the binding specificity analysis, cells were initially exposed to $Z_{HER2:342}$ (10 μM) for 1 h before being treated with Cy5.5-labeled Z-E ADCN (10 μM) for another 4 h, after which they were collected and analyzed using FCM.

In the confocal laser scanning microscopy (CLSM) study, SKOV-3 cells were seeded at a density of 2×10^5 cells per well and allowed to grow overnight. Subsequently, Cy5.5-labeled Z-E ADCN was added at a concentration of 10 μM, and the cells were incubated for specific time intervals at 37 °C. Following this, the cell nuclei were stained with Hoechst 33,342 before observation using confocal microscope.

Cytotoxicity evaluation

Different cells were seeded at a density of 5×10^3 cells per well and incubated overnight, respectively. After that, Epo B or Z-E ADCN were added at different concentrations. Following another 48-hour incubation, CCK-8 solution was added and the absorbance at 450 nm was measured by a BioTek Synergy H4 system.

Apoptosis analyses

The SKOV-3 cells were seeded at a density of 5×10^5 cells per well and incubated overnight. Then free Epo B and Z-E ADCN at a concentration of 30 nM were added and incubated for another 24 h, respectively. Finally, the cells were subjected to staining and then analyzed using FCM.

Construction of tumor models

The nude mice were subcutaneously injected with 200 μL of cell suspension containing 3×10^6 SKOV-3 cells in the right flank region. The tumors were allowed to reach a size of around 100 mm^3 before starting the antitumor experiments.

Pharmacokinetics

Sprague-Dawley rats (~200 g) were randomly assigned to receive either Cy5.5-labeled $Z_{HER2:342}$ or Cy5.5-labeled Z-E ADCN (n=4). Both compounds were administered intravenously via the tail vein. Blood samples were collected at predetermined time interval through eye puncture. The fluorescence intensity of serum was measured using a BioTek Synergy H4 system. The concentrations of both compounds were determined based on their standard curves.

Biodistribution analysis.

As to the in vivo optical imaging study, SKOV-3 tumor-bearing mice were randomly assigned to three groups and treated with 200 μL of free Cy5.5, Cy5.5-labeled $Z_{HER2:342}$ or Cy5.5-labeled Z-E ADCN, respectively. The fluorescence distribution was assessed at predetermined time interval through multimode imaging system.

For the ex vivo biodistribution study, 200 μL of different compounds were injected into tumor-bearing nude mice, respectively. Subsequently, tumors and major organs were harvested at 1, 4 and 8 h post-injection with careful handling. Following PBS rinsing, immediate imaging was conducted for all samples.

Antitumor activity

The SKOV-3 tumor-bearing mice were randomly allocated into four groups ($n=5$) and treated with PBS, $Z_{HER2:342}$ (139 mg kg^{-1}), Epo B (5 mg kg^{-1}), Z-E ADCN (78 mg kg^{-1}, an equivalent dose of Epo B at 5 mg kg^{-1}) and Z-E ADCN (156 mg kg^{-1}, an equivalent dose of Epo B at 10 mg kg^{-1}) once every 3 days for 24 days, respectively. The body weight and tumor volume were measured with each injection. Tumor volume was calculated using the formula: $V=1/2\times length\times width^2$. After a total of eight injections, the mice were sacrificed and their tumors and major organs were collected for further analysis.

Statistical analysis

The acquired data were presented as mean±SD. Statistical significance of each group was analyzed using Student's t-test calculated by prism software, with $P<0.05$ indicating statistical significance.

Results and discussion

Synthesis and characteristics of Z-E ADCN

The recombinant affibody molecule $Z_{HER2:342}$-Cys-EK-His(MGHHHHHHHHHHSSGHIDDDDKHMCVDNKFNKEMRNAYWEIALLPNLNNQQKRAFIRSLYDDPSQSANLLAEAKKLNDAQAPK) as shown in Fig. S1 was first expressed in *Escherichia coli* and purified using the Ni-nitrilotriacetyl agarose column. The molecular weight of $Z_{HER2:342}$-Cys-EK-His was confirmed by MALDI-TOF-MS, showing two peaks at 9707.39 (monomer) and 19415.42 Da (dimer), which closely matched the theoretical mass of 9707.63 and 19412.25 Da, respectively (Fig. S2). Subsequently, His-tag was removed through the enterokinase mediated cleavage to obtain $Z_{HER2:342}$-Cys, as depicted in Fig. 1A, with a detected mass of 7076.92 (monomer) and 14153.01 Da (dimer), in good agreement with the theoretical mass of 7077.83 and 14153.66 Da, confirming the successful preparation of $Z_{HER2:342}$-Cys.

The Epo B-tk-MAL compound was initially synthesized according to our previous methodology (Fig. S3) [26]. Subsequently, a dimethyl sulfoxide solution of Epo B-tk-MAL was added dropwise to the $Z_{HER2:342}$-Cys solution to form the $Z_{HER2:342}$-Epo B conjugate via thiol-maleimide click chemistry (Fig. S4). MALDI-TOF-MS result of the purified solution in Fig. 1B revealed a single peak at 7940.55, which is in line with the theoretical mass of the $Z_{HER2:342}$-Epo B conjugate (7942.21). Due to its inherent amphiphilic structure, the resulting conjugate can self-assemble into $Z_{HER2:342}$-Epo B Affibody Drug Conjugate Nanoagent (Z-E ADCN). As shown in Fig. 1C, the dynamic light scattering (DLS) analysis of Z-E ADCN revealed the presence of aggregates with a narrow distribution and an average hydrodynamic diameter of approximately 75.01 nm. Transmission electron microscopy (TEM) images in Fig. 1D also distinctly exhibited spherical morphology with size about 72.5 nm, consistent with the DLS results. Meanwhile, we also investigated the morphologies of $Z_{HER2:342}$-Cys and Epo B-MAL,

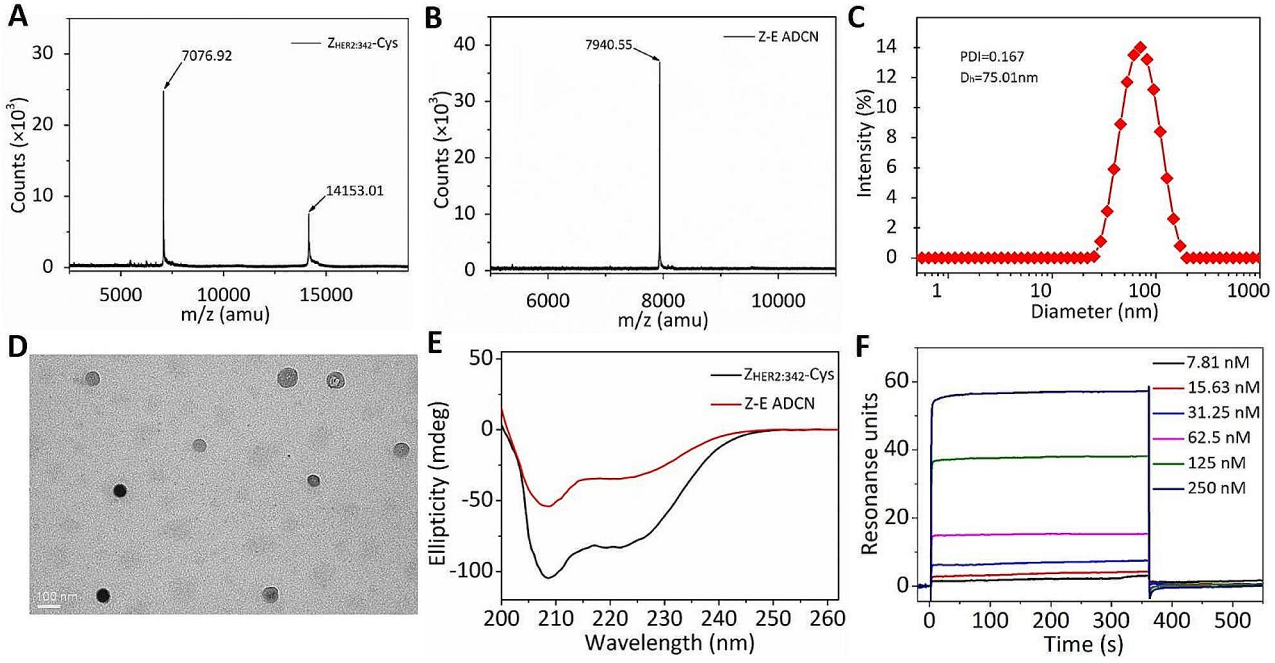

Fig. 1 Characterizations of $Z_{HER2:342}$-Cys and Z-E ADCN (**A**-**B**) MALDI-TOF-MS result of $Z_{HER2:342}$-Cys and Z-E ADCN. (**C**) DLS result of Z-E ADCN. (**D**) TEM image of Z-E ADCN. Scale bars: 100 nm. (**E**) CD spectrum of $Z_{HER2:342}$-Cys and Z-E ADCN. (**F**) The affinity analysis result about Z-E ADCN with extracellular domain (ECD) of HER2.

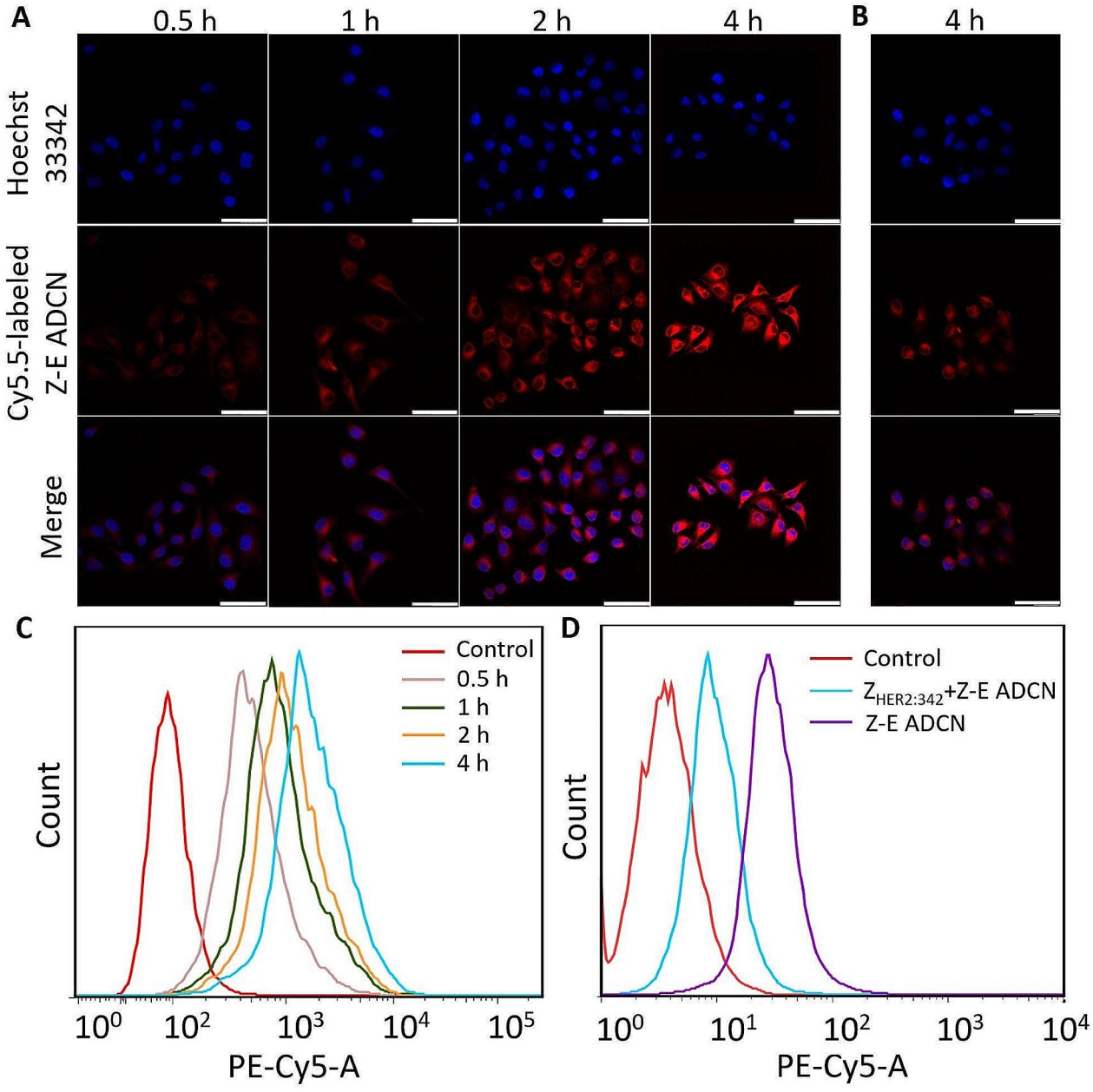

Fig. 2 In vitro cellular uptake behavior of Z-E ADCN (**A**) CLSM images depict the uptake of Z-E ADCN labeled with Cy5.5 by SKOV-3 cells at different time points, with cell nuclei stained using Hoechst 33,342. (**B**) CLSM images showing the co-incubation of SKOV-3 cells with $Z_{HER2:342}$ (10 μM) for 1 h followed by incubation with Z-E ADCN labeled with Cy5.5 for an additional 4 h. Scale bars: 25 μm. (**C**) FCM analysis of the in vitro cellular uptake behaviors of Cy5.5-labeled Z-E ADCN at specified time intervals. (**D**) FCM assessment of SKOV-3 cells following incubation with or without $Z_{HER2:342}$ (10 μM) for 1 h and subsequent incubation with Z-E ADCN labeled with Cy5.5 (10 μM) for another 4 h

respectively, and only found random irregular aggregates in the TEM images as shown in Fig. S5. Furthermore, the zeta potential measurement (Fig. S6) indicated a negative-charged surface of Z-E ADCN with a value of -3.9 mV, which is attributed to the high density of affibody corona on the particles. Additionally, the average diameter and size distribution of Z-E ADCN exhibited no significant changes over a period of 3 weeks, demonstrating its high storage stability (Fig. S7). Importantly, the diameter of Z-E ADCN in water with 5 or 10% FBS exhibited consistent stability, indicating its superior serum stability (Fig. S8). All these data demonstrate the successful preparation of Z-E ADCN.

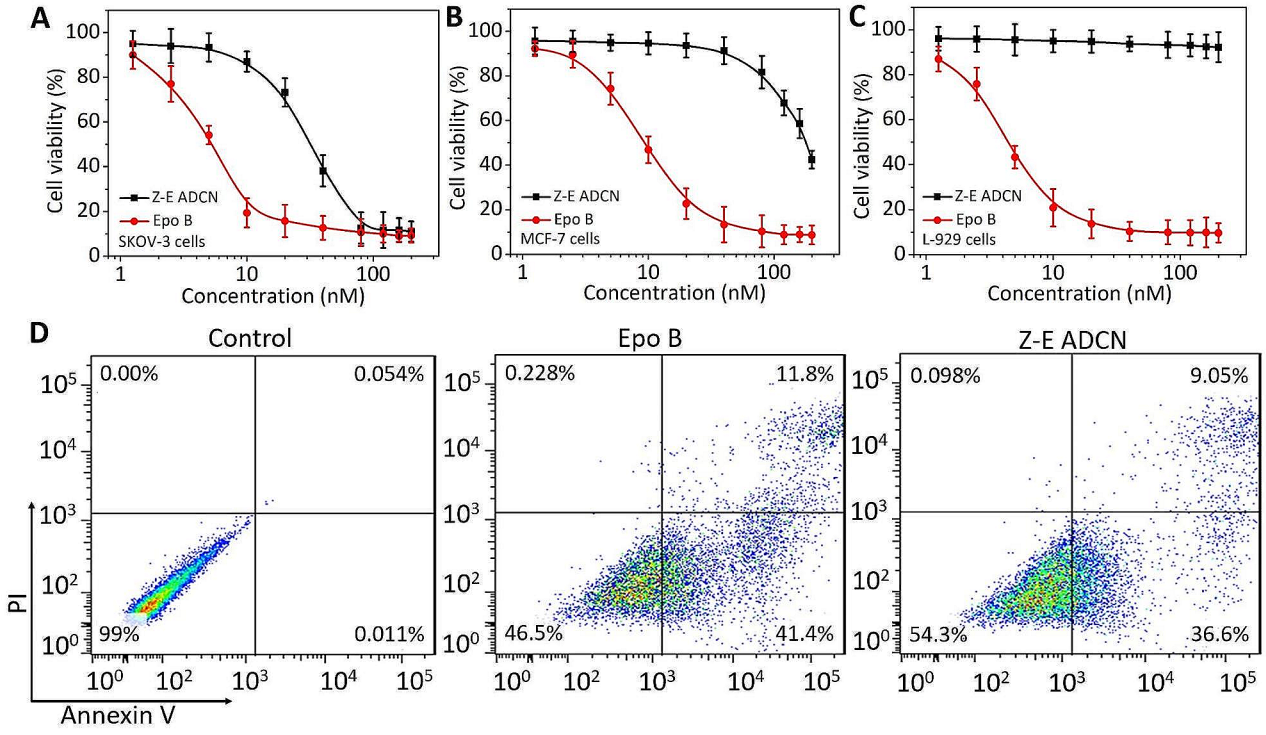

Fig. 3 Relative cell viabilities of SKOV-3 (**A**), MCF-7 (**B**), and L929 (**C**) cells following a 48-hour incubation with free Epo B or Z-E ADCN. The data are presented as the average ± standard error ($n = 6$). (**D**) FCM analysis was performed to assess the apoptosis of SKOV-3 cells induced by various compounds. Lower left, living cells; lower right, early apoptotic cells; upper right, late apoptotic cells; upper left, necrotic cells

Affinity analysis

The outstanding affinity performance of affibody is closely associated with their α-helical conformation [37, 38]. Thus, circular dichroism (CD) measurement was first performed to confirm whether the helical structure of $Z_{HER2:342}$ in Z-E ADCN kept unchanged. As shown in Fig. 1E, distinct negative peaks at 208 and 222 nm were observed in both Z-E ADCN and $Z_{HER2:342}$ groups, confirming that α-helical secondary structure is still dominating in $Z_{HER2:342}$ of Z-E ADCN. Subsequently, biospecific affinity analysis between $Z_{HER2:342}$ (or Z-E ADCN) and HER2-ECD was carried out. As expected, both $Z_{HER2:342}$ and Z-E ADCN were found binding to HER2 with high affinity (Fig. 1F and Table S1). The association rate constant (k_a) of Z-E ADCN was determined as 4.16×10^4 M^{-1} s^{-1}, slightly elevated compared to that of $Z_{HER2:342}$ as 6.11×10^3 M^{-1} s^{-1}, which is likely ascribed to the abundance of $Z_{HER2:342}$ molecules on the surface of Z-E ADCN. Moreover, the dissociation rate constant (k_d) of Z-E ADCN was found to be 1.75×10^{-3} s^{-1}, faster than that of $Z_{HER2:342}$ at 1.67×10^{-6} s^{-1}. These data resulted in a dissociation equilibrium constant (K_D) for Z-E ADCN of 4.21×10^{-8} M, which is marginally higher than that for $Z_{HER2:342}$ at 2.74×10^{-10} M. The ascension of dissociation rate constant may be caused by the relatively large size of Z-E ADCN, but for all that, the binding affinity remains within nanomolar range, exhibiting enough sensitivity for targeted therapy applications [39].

ROS responsiveness of Z-E ADCN

The thioketal (tk) group has been shown to exhibit reactivity towards the elevated levels of reactive oxygen species (ROS) present in cancer cells, as confirmed by previous studies. [26, 40]. In order to ascertain the potential release of Epo B from Z-E ADCN via tk degradation within cancer cells, we conducted an investigation of intracellular degradation. First, SKOV-3 cells (with high HER2 expression [41] and high level of ROS [42]) were treated with Z-E ADCN for 8 h, then the cellular extracts were collected and measured by LC-MS technique. Standard Epo B was used as the control. As shown in Fig. S9, the molecular weight and retention time for standard Epo B are 508.2751 Da and 5.92 min, respectively. As expected, free Epo B was found to be present in the cell extracts, corresponding to molecular weight and retention time of 508.2739 Da and 5.92 min, respectively, confirming that free Epo B can be released in cancer cells. All these LC-MS results verify that Z-E ADCN can be degraded to release Epo B after internalization of cancer cells.

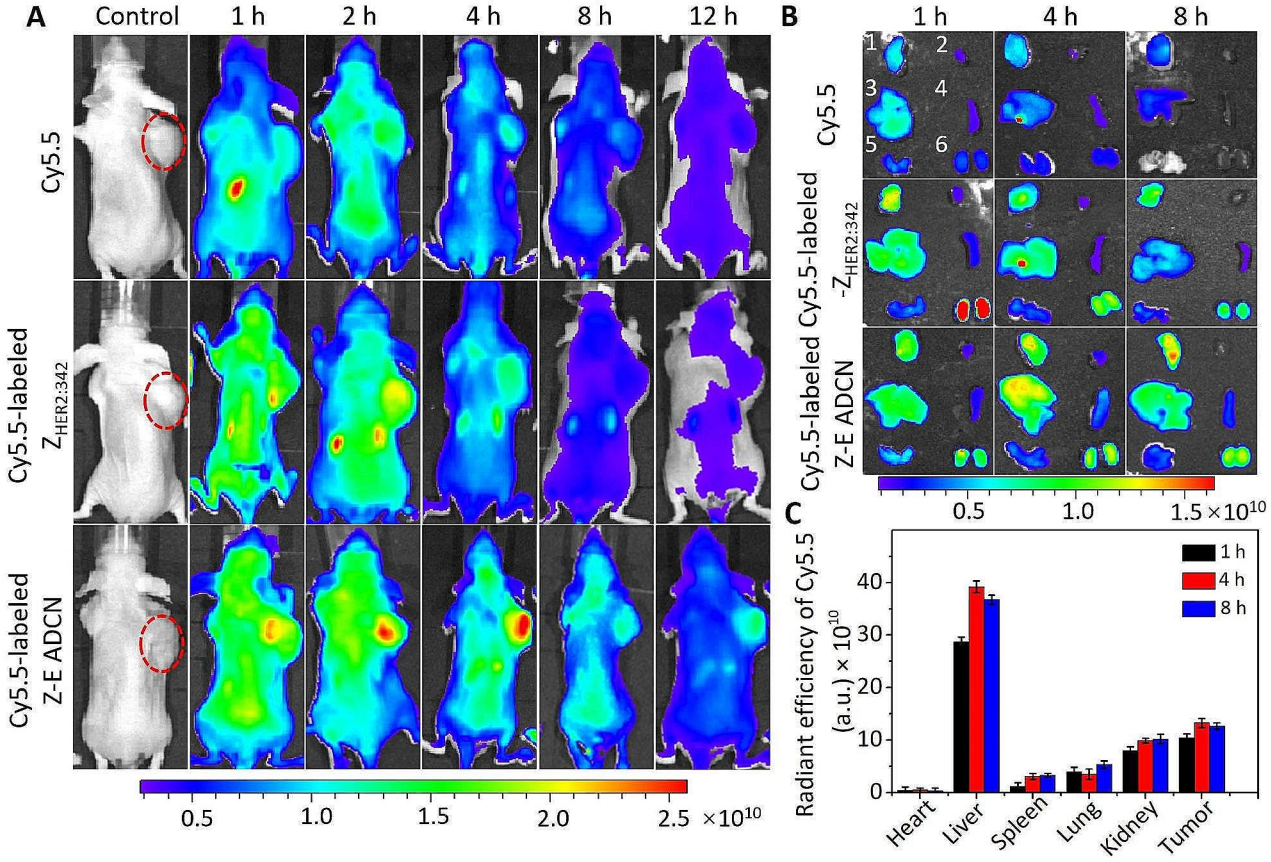

Fig. 4 The biodistribution of Z-E ADCN in mice following treatment. (**A**) In vivo visualization of mice treated with free Cy5.5, Cy5.5-labeled $Z_{HER2:342}$, Cy5.5-labeled Z-E ADCN. The areas of tumor presence are outlined by red dashed lines. (**B**) Fluorescent images of various tissues obtained from mice after different treatments. Tissues included tumor (1), heart (2), liver (3), spleen (4), lung (5), and kidneys (6). (**C**) Quantitative analysis of tissue distribution of Cy5.5-labeled Z-E ADCN at 1 h, 4 h, and 8 h post injection. Data are presented as average ± standard error ($n = 4$)

In Vitro Analysis of Z-E ADCN

For the investigation of cellular uptake behavior, Z-E ADCN was conjugated with Cy5.5 dye to produce Cy5.5-labeled Z-E ADCN. The morphological properties of the Cy5.5-labeled Z-E ADCN were found to be consistent with those of the original Z-E ADCN, as demonstrated in Fig. S10. Subsequently, SKOV-3 cells were exposed to Z-E ADCN labeled with Cy5.5 for a prearranged period and then analyzed using FCM and CLSM. As depicted in Fig. 2A and C, the fluorescence signal in cells significantly increased with prolonged incubation time. In addition, red fluorescence emitted by Cy5.5 was observed in both cytoplasm and nuclei after 4 h incubation, indicating the effective internalization of Z-E ADCN by SKOV-3 cells. To further explore the HER2-specific endocytosis of Z-E ADCN by SKOV-3 cells, the cells were first treated with $Z_{HER2:342}$ for 1 h followed by culture with Cy5.5-labeled Z-E ADCN for an additional 4 h. Direct incubation of cells with Cy5.5-labeled Z-E ADCN was used as control. The CLSM images and FCM data are presented in Fig. 2B and D, respectively, where we can see that the internalization of Z-E ADCN is significantly suppressed following pre-incubation with free $Z_{HER2:342}$, suggesting that the interaction between Z-E ADCN and SKOV-3 cells is mediated by HER2-specific receptor binding.

Previous studies have demonstrated that the cytotoxicity of affibody-drug constructs is contingent upon the level of HER2 expression [38, 43, 44]. Additionally, the incorporation of tk group in prodrug has been shown to induce selective cytotoxicity towards cancer cells compared to normal cells, probably attributed to the elevated levels of ROS in cancer cells [26]. Therefore, it was hypothesized that Z-E ADCN would demonstrate specific cytotoxicity against cells with different levels of HER2 expression and ROS. To prove that, in vitro cytotoxicity of Z-E ADCN and free Epo B were assessed on SKOV-3 cells, MCF-7 cells (low HER2 but high ROS expression), and L929 cells (low HER2 and ROS expression). As shown in Fig. 3A and C, the IC_{50} of free Epo B in SKOV-3 cells is 5.22 nM, which is not significantly different from that in MCF-7 cells (8.9 nM) and L929 cells (4.51 nM), indicating non-selectivity of Epo B towards these cell types. In contrast, Z-E ADCN showed a potent cytotoxic effect on SKOV-3 cells with an IC_{50} value of

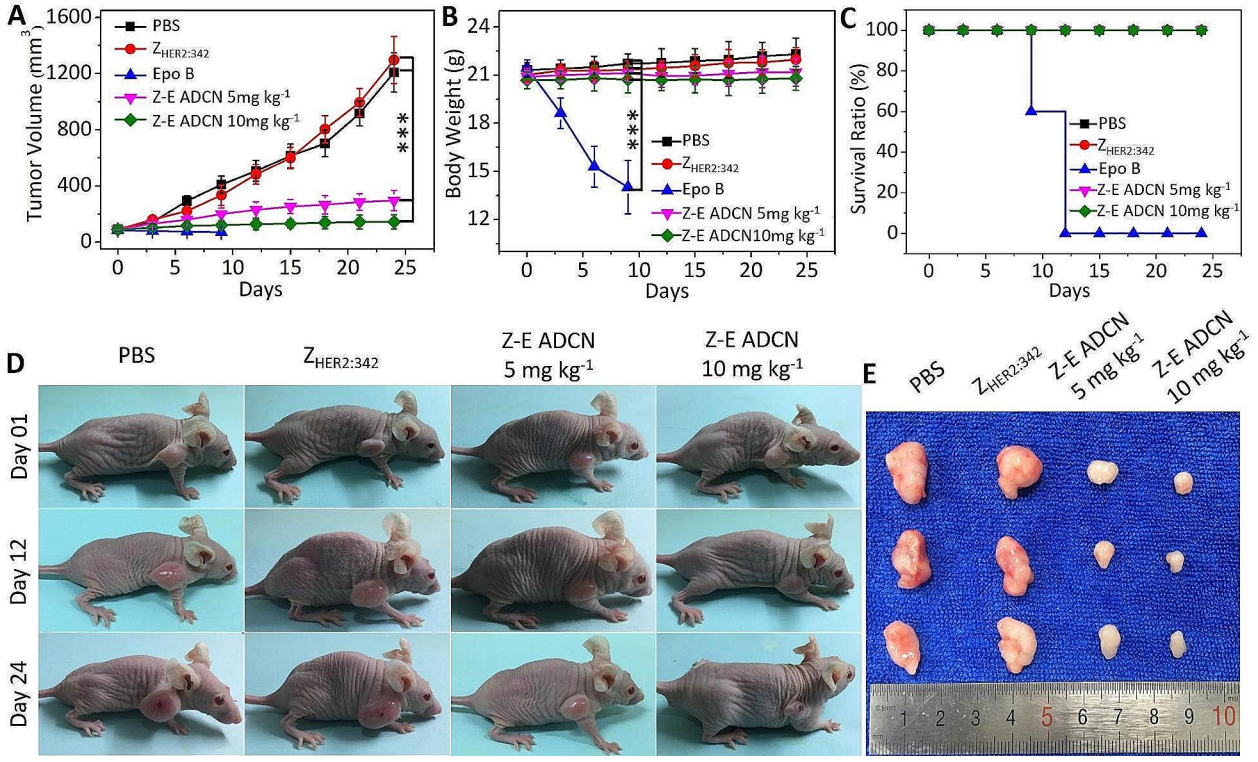

Fig. 5 In vivo assessment of the therapeutic efficacy of Z-E ADCN as antitumor agents. (**A**) Tumor volumes in each treatment group following intravenous administration of PBS, $Z_{HER2:342}$, Epo B, and Z-E ADCN ($n = 5$ per group). Statistical significance; $^{*}P < 0.05$, $^{**}P < 0.01$, and $^{***}P < 0.001$. (**B**) Changes in body weight of tumor-bearing mice post-treatment. (**C**) Survival curves of tumor-bearing mice with indicated treatments. (**D**) Photographic documentation of tumor-bearing mice at day 1, day 12 and day 24 post-treatment. (**E**) Representative images of the harvested tumors after a treatment period of 24 days

31.06 nM, while for MCF-7 cells the IC_{50} value increased to 183.77 nM and had no effect on L929 cells at the tested concentrations. These results definitely suggest that Z-E ADCN exhibits significantly specific toxicity against cancer cells with elevated levels of HER2 expression and ROS, which is most likely caused by the HER2 targeted property of $Z_{HER2:342}$ affibody and the ROS-triggered release of Epo B.

Additionally, a cell apoptosis study was also carried out and examined through FCM. SKOV-3 cells were exposed to PBS, Epo B, and Z-E ADCN for a duration of 24 h, respectively. As shown in Fig. 3D, the percentage of apoptotic cells induced by Epo B and Z-E ADCN is 53.5% and 45.7%, respectively, suggesting that Z-E ADCN exhibits a comparable capacity to Epo B in inducing cellular apoptosis.

Pharmacokinetic and Biodistribution studies

Previous studies have demonstrated that the free affibody has a relatively short half-life because of its low molecular weight. [45, 46]. Therefore, the pharmacokinetics study of Z-E ADCN was conducted through intravenous injection of Cy5.5-labeled Z-E ADCN into SD rats, and the drug concentration was calculated according to the standard concentration-absorbance curve of Cy5.5-labeled $Z_{HER2:342}$ (Fig. S11). As depicted in Fig. S12, the metabolic rate of Z-E ADCN is notably slower than that of $Z_{HER2:342}$. The concentration of Z-E ADCN in the bloodstream remains relatively high at 5.6 μg mL^{-1} after 12 h post-injection, whereas the concentration of free $Z_{HER2:342}$ is only 0.4 μg mL^{-1} at the same time point. Compared to free $Z_{HER2:342}$, the prolonged circulation of Z-E ADCN could potentially increase the accumulation of HER2-specific drugs in tumor tissue. To demonstrate the HER2-specific tumor-targeting capability of Z-E ADCN, in vivo fluorescence imaging was also conducted in nude mice with SKOV-3 tumors. As depicted in Fig. 4A, the fluorescence signal of Cy5.5-labeled $Z_{HER2:342}$ and free Cy5.5 groups decreases rapidly from 1 to 12 h post-injection, which is probably due to their small molecular sizes. In contrast, the Cy5.5-labeled Z-E ADCN group exhibits a consistently strong fluorescence signal, particularly in tumor tissue. These findings suggest that Z-E ADCN has a prolonged blood retention time and can effectively accumulate at the tumor site.

To further study the biodistribution of Z-E ADCN, SKOV-3 tumor-bearing mice were sacrificed and their tumors and major organs were collected for ex vivo imaging and quantitative analysis at 1, 4, and 8 h after injection. As depicted in Fig. 4B and C, the fluorescence signal

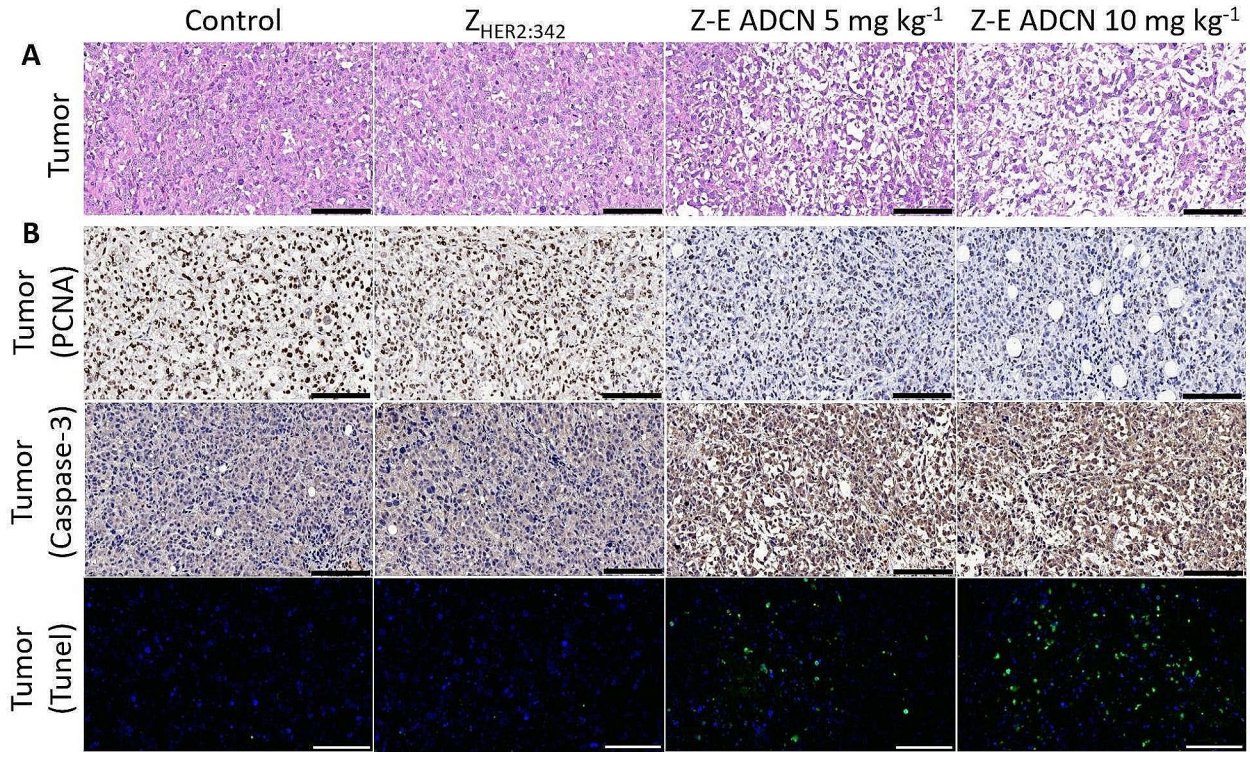

Fig. 6 Immunohistochemical analysis results of tumor from different treatment groups. (**A**-**B**) H&E staining, proliferating cell nuclear antigen (PCNA), Caspase-3 and Tunel staining of tumor tissues after indicated treatments. Scale bars: 100 μm

of Z-E ADCN accumulates predominantly in tumor, liver, and kidney tissues, with relatively stable levels observed from 1 to 8 h post-injection. Notably, the fluorescence signal of Z-E ADCN within the tumor site is significantly stronger than that of $Z_{HER2:342}$ and free Cy5.5 groups, indicating its exceptional active tumor targeting performance. All these results collectively suggest that Z-E ADCN exhibits outstanding tumor targeting capabilities with promising potential for cancer therapy.

In Vivo Antitumor Studies

Building on its outstanding targeting property, in vivo antitumor assessment of Z-E ADCN was further conducted. The mice with SKOV-3 tumor were randomly allocated into five groups and administered with PBS, $Z_{HER2:342}$, Epo B (5 mg kg^{-1}), Z-E ADCN (at 5 mg kg^{-1} or 10 mg kg^{-1} Epo B-equivalent dose) every 3 days for 24 days, respectively. As shown in Fig. 5A, treatment with Z-E ADCN at a 5 mg kg^{-1} Epo B-equivalent dose effectively inhibited tumor growth, and the growth tendency was almost totally suppressed when the dose increased to 10 mg kg^{-1}. Notably, due to severe side effects of Epo B, mice treated with free Epo B at 5 mg kg^{-1} experienced significant weight loss (Fig. 5B) and all animals in this cohort perished after four administrations (Fig. 5C), resulting in an absence of therapeutic data within this group (Fig. 5A). Whereas, even in the Z-E ADCN group (10 mg kg^{-1} Epo B-equivalent dose), the body weights of mice only exhibited a slight decrease compared to that of the control group, indicating minimal side effects of Z-E ADCN (Fig. 5D), which was probably due to its controlled drug release property. Furthermore, following completion of the treatment regimen, the mice were euthanized and tumors were collected and photographed (Fig. 5E). The tumor weight was documented to determine the tumor inhibitory rate (TIR) as shown in Fig. S13. In comparison to the PBS group, the TIR of $Z_{HER2:342}$ is negligible at 1.6%, significantly lower than that of Z-E ADCN (5 and 10 mg kg^{-1} Epo B-equivalent dose) at 77.9% and 89.3%, respectively, verifying its outstanding tumor inhibition ability. All above results indicate that Z-E ADCN exhibits superior biosecurity and outstanding antitumor performance.

Immunohistochemical Analysis

Histological and immunohistochemical analysis of the tumor were performed after the whole treatment. As depicted in Fig. S14, the hematoxylin and eosin (H&E) staining assay of major organs revealed no discernible differences between Z-E ADCN treated and the control groups, indicating minimal side effects of Z-E ADCN. Furthermore, Z-E ADCN effectively induced apoptosis in tumor tissues compared to the PBS or $Z_{HER2:342}$ treated groups, as evidenced by extensive nuclear shrinkage and

fragmentation shown in Fig. 6A. Additionally, the immunohistochemical analysis results in Fig. 6B demonstrated that Z-E ADCN not only inhibited cancer cell proliferation, as indicated by significantly reduced expression of proliferating cell nuclear antigen (PCNA), but also induced more efficient apoptosis in tumor tissues, as evidenced by enhanced expression levels of caspase-3 and TUNEL. The above findings further demonstrate the minimal occurrence of adverse effects and the superior in vivo antitumor efficacy of our Z-E ADCN.

Conclusions

In summary, we have developed a targeted nano-delivery system for cancer therapy by combining affibody with anticancer drug. The data evidently demonstrate the successful construction of Z-E ADCN by molecular self-assembly from the $Z_{HER2:342}$-Epo B conjugate. Z-E ADCN can specifically bind to HER2 and enter the cell via HER2-mediated endocytosis, after which Epo B can be released through the degradation of tk group due to elevated ROS levels in cancer cells. Furthermore, the nanoscale properties of Z-E ADCN can also lead to prolonged circulating times in the bloodstream, increased drug accumulation in tumors, and reduced adverse effects on normal organs. These factors collectively contribute to the enhanced antitumor efficacy of Z-E ADCN in vitro and in vivo. All in all, our self-assembly approach offers a promising avenue for the application of Epo B in clinics. Looking ahead, we anticipate that our strategy can be further expanded to encompass a wide range of affibody molecules combined with various anticancer agents for the treatment of different cancers.

Supplementary Information

The online version contains supplementary material available at https://doi.org/10.1186/s12951-024-02754-4.

Supplementary Material 1

Acknowledgements
Not applicable.

Author contributions
D.Y. and X.X. (Xuelin Xia) conceived the project. X.X. (Xuelin Xia) designed, conducted the experiments and drafted the manuscript. X.X. (Xiaoxia Xia), W.G. and X.Y. provided technical support for the experiments and contributed to the investigations. D.Y., X.X. (Xiaoxia Xia) and W.H. provided oversight for this study and made revisions of the manuscript. All authors conducted a thorough review of the article and gave their approval for the final manuscript.

Funding
This work was supported by the National Natural Science Foundation of China (22201178, 52273281) and the Medical Engineering Cross Project of Shanghai Jiao Tong University (YG2019ZDA05, YG2021QN35).

Data availability
No datasets were generated or analysed during the current study.

Declarations

Ethics approval and consent to participate
All animal experiments were approved by the Animal Ethical Committee of Shanghai Jiao Tong University. All procedures were in compliance with the relevant guidelines and regulations.

Consent for publication
Not applicable.

Competing interests
The authors declare no competing interests.

Received: 13 June 2024 / Accepted: 5 August 2024
Published online: 21 August 2024

References

1. Bollag DM, McQueney PA, Zhu J, Hensens O, Koupal L, Liesch J, et al. Epothilones, a new class of microtubule-stabilizing agents with a taxol-like mechanism of action. Cancer Res. 1995;55:2325–33.
2. Höfle G, Bedorf N, Steinmetz H, Schomburg D, Gerth K, Reichenbach H. Epothilone A and B—novel 16-membered macrolides with cytotoxic activity: isolation, crystal structure, and conformation in solution. Angew Chem Int Ed. 1996;35:1567–9.
3. Nicolaou KC, Rhoades D, Wang Y, Bai R, Hamel E, Aujay M, et al. 12, 13-Aziridinyl epothilones. Stereoselective synthesis of trisubstituted olefinic bonds from methyl ketones and heteroaromatic phosphonates and design, synthesis, and biological evaluation of potent antitumor agents. J Am Chem Soc. 2017;139:7318–34.
4. Giannakakou P, Gussio R, Nogales E, Downing KH, Zaharevitz D, Bollbuck B, et al. A common pharmacophore for epothilone and taxanes: molecular basis for drug resistance conferred by tubulin mutations in human cancer cells. Proc Natl Acad Sci USA. 2000;97:2904–9.
5. Zhang P, Zhang L, Jiang X, Diao XT, Li S, Li DD. Docking-guided rational engineering of a macrolide glycosyltransferase glycodiversifies epothilone B. Commun Biol. 2022;5:100.
6. Chiorazzi A, Nicolini G, Canta A, Oggioni N, Rigolio R, Cossa G, et al. Experimental epothilone B neurotoxicity: results of in vitro and in vivo studies. Neurobiol Dis. 2009;35:270–7.
7. Lee FY, Borzilleri R, Fairchild CR, Kim SH, Long BH, Reventos-Suarez C, et al. BMS-247550: a novel epothilone analog with a mode of action similar to paclitaxel but possessing superior antitumor efficacy. Clin Cancer Res. 2001;7:1429–37.
8. Pronzato P. New therapeutic options for chemotherapy-resistant metastatic breast cancer: the epothilones. Drugs. 2008;68:139–46.
9. Clinical trial data. for ABJ879 (Novartis) was not publicly disclosed.
10. Sessa C, Perotti A, Llado A, Cresta S, Capri G, Voi M, et al. Phase I clinical study of the novel epothilone B analogue BMS-310705 given on a weekly schedule. Ann Oncol. 2007;18:1548–53.
11. Kaur J, Gulati M, Jha NK, Disouza J, Patravale V, Dua K, et al. Recent advances in developing polymeric micelles for treating cancer: breakthroughs and bottlenecks in their clinical translation. Drug Discov Today. 2022;27:1495–512.
12. Zhou Q, Shao S, Wang J, Xu C, Xiang J, Piao Y, et al. Enzyme-activatable polymer-drug conjugate augments tumour penetration and treatment efficacy. Nat Nanotechnol. 2019;14:799–809.
13. Sun C, Lu J, Wang J, Hao P, Li C, Qi L, et al. Redox-sensitive polymeric micelles with aggregation-induced emission for bioimaging and delivery of anticancer drugs. J Nanobiotechnol. 2021;19:1–15.
14. Liang X, Shi B, Wang K, Fan M, Jiao D, Ao J, et al. Development of self-assembling peptide nanovesicle with bilayers for enhanced EGFR-targeted drug and gene delivery. Biomaterials. 2016;82:194–207.
15. Ao H, Wang Z, Lu L, Ma H, Li H, Fu J, et al. Enhanced tumor accumulation and therapeutic efficacy of liposomal drugs through over-threshold dosing. J Nanobiotechnol. 2022;20:1–14.
16. Shen Y, Jin E, Zhang B, Murphy CJ, Sui M, Zhao J, et al. Prodrugs forming high drug loading multifunctional nanocapsules for intracellular cancer drug delivery. J Am Chem Soc. 2010;132:4259–65.
17. Pan S, Zhang Y, Natalia A, Lim CZ, Ho NR, Chowbay B, et al. Extracellular vesicle drug occupancy enables real-time monitoring of targeted cancer therapy. Nat Nanotechnol. 2021;16:734–42.

18. Wang J, Hu S, Mao W, Xiang J, Zhou Z, Liu X, et al. Assemblies of peptide-cytotoxin conjugates for tumor-homing chemotherapy. Adv Funct Mater. 2019;29:1807446.
19. Li F, Liang Y, Wang M, Xu X, Zhao F, Wang X, et al. Multifunctional nanoplatforms as cascade-responsive drug-delivery carriers for effective synergistic chemo-photodynamic cancer treatment. J Nanobiotechnol. 2021;19:1–18.
20. Smith BA, Bertozzi CR. The clinical impact of glycobiology: targeting selectins, siglecs and mammalian glycans. Nat Rev Drug Discov. 2021;20:217–43.
21. Moghaddam FD, Heidari G, Zare EN, Djatoubai E, Paiva-Santos AC, Bertani FR, et al. Carbohydrate polymer-based nanocomposites for breast cancer treatment. Carbohydr Polym. 2023;304:120510.
22. Silant' ev VE, Shmelev ME, Belousov AS, Patlay AA, Shatilov RA, Farniev VM, et al. How to develop drug delivery system based on carbohydrate nanoparticles targeted to brain tumors. Polymers. 2023;15:2516.
23. Casi G, Neri D. Antibody-drug conjugates and small molecule-drug conjugates: opportunities and challenges for the development of selective anticancer cytotoxic agents. J Med Chem. 2015;58:8751–61.
24. Chen YT, Luo YX, Chan SH, Chiu WY, Yang HW. Dual antibody-aided mesoporous nanoreactor for H_2O_2 self-supplying chemodynamic therapy and checkpoint blockade immunotherapy in triple-negative breast cancer. J Nanobiotechnol. 2023;21:1–16.
25. Xu Y, Qian L, Fang M, Liu Y, Xu ZJ, Ge X, et al. Tumor selective self-assembled nanomicelles of carbohydrate-epothilone B conjugate for targeted chemotherapy. Eur J Med Chem. 2023;259:115693.
26. Xia X, Yang X, Huang P, Yan D. ROS-Responsive nanoparticles formed from RGD – epothilone B conjugate for targeted cancer therapy. ACS Appl Mater Interfaces. 2020;12:18301–8.
27. Nord K, Gunneriusson E, Ringdahl J, Ståhl S, Uhlén M, Nygren PÅ. Binding proteins selected from combinatorial libraries of an α-helical bacterial receptor domain. Nat Biotechnol. 1997;15:772–7.
28. Orlova A, Magnusson M, Eriksson TL, Nilsson M, Larsson B, Höidén-Guthenberg I, et al. Tumor imaging using a picomolar affinity HER2 binding affibody molecule. Cancer Res. 2006;66:4339–48.
29. Ståhl S, Gräslund T, Karlström AE, Frejd FY, Nygren PÅ, Löfblom J. Affibody molecules in biotechnological and medical applications. Trends Biotechnol. 2017;35:691–712.
30. Luo R, Liu H, Cheng Z. Protein scaffolds: antibody alternatives for cancer diagnosis and therapy. RSC Chem Biol. 2022;3:830–47.
31. Gao W, Xia X, Yang X, Li Q, Xia X, Huang W, et al. Amphiphilic Affibody-PROTAC conjugate self-assembled nanoagents for targeted cancer therapy. Chem Eng J. 2024;495:153437.
32. Xia X, Yang X, Huang W, Xia X, Yan D. Self-assembled nanomicelles of affibody-drug conjugate with excellent therapeutic property to cure ovary and breast cancers. Nano-Micro Lett. 2022;14:33.
33. Yang X, Xia X, Huang W, Xia X, Yan D. Highly efficient tumor-targeted nanomedicine assembled from affibody-drug conjugate for colorectal cancer therapy. Nano Res. 2023;16:5256–64.
34. Chen D, Zhang G, Li R, Guan M, Wang X, Zou T, et al. Biodegradable, hydrogen peroxide, and glutathione dual responsive nanoparticles for potential programmable paclitaxel release. J Am Chem Soc. 2018;140:7373–6.
35. Hu JJ, Lei Q, Peng MY, Zheng DW, Chen YX, Zhang XZ. A positive feedback strategy for enhanced chemotherapy based on ROS-triggered self-accelerating drug release nanosystem. Biomaterials. 2017;128:136–46.
36. Wilson DS, Dalmasso G, Wang L, Sitaraman SV, Merlin D, Murthy N. Orally delivered thioketal nanoparticles loaded with TNF-α – siRNA target inflammation and inhibit gene expression in the intestines. Nat Mater. 2010;9:923–8.
37. Eigenbrot C, Ultsch M, Dubnovitsky A, Abrahmsén L, Härd T. Structural basis for high-affinity HER2 receptor binding by an engineered protein. Proc Natl Acad Sci USA. 2010;107:15039–44.
38. Altai M, Liu H, Ding H, Mitran B, Edqvist PH, Tolmachev V, et al. Affibody-derived drug conjugates: potent cytotoxic molecules for treatment of HER2 over-expressing tumors. J Control Release. 2018;288:84–95.
39. Srinivasarao M, Galliford CV, Low PS. Principles in the design of ligand-targeted cancer therapeutics and imaging agents. Nat Rev Drug Discov. 2015;14:203–19.
40. Rinaldi A, Caraffi R, Grazioli MV, Oddone N, Giardino L, Tosi G, et al. Applications of the ROS-responsive thioketal linker for the production of smart nanomedicines. Polymers. 2022;14:687.
41. Hoppmann S, Miao Z, Liu S, Liu H, Ren G, Bao A, et al. Radiolabeled affibody-albumin bioconjugates for HER2-positive cancer targeting. Bioconjug Chem. 2011;22:413–21.
42. Szatrowski TP, Nathan CF. Production of large amounts of hydrogen peroxide by human tumor cells. Cancer Res. 1991;51:794–8.
43. Sochaj-Gregorczyk AM, Serwotka-Suszczak AM, Otlewski J. A novel affibody-auristatin e conjugate with a potent and selective activity against HER2 + cell lines. J Immunother. 2016;39:223–32.
44. Serwotka-Suszczak AM, Sochaj-Gregorczyk AM, Pieczykolan J, Krowarsch D, Jelen F, Otlewski J. A conjugate based on anti-HER2 diaffibody and auristatin E targets HER2-positive cancer cells. Int J Mol Sci. 2017;18:401.
45. Beuttler J, Rothdiener M, Müller D, Frejd FY, Kontermann RE. Targeting of epidermal growth factor receptor (EGFR)-expressing tumor cells with sterically stabilized affibody liposomes (SAL). Bioconjug Chem. 2009;20:1201–8.
46. Seijsing J, Lindborg M, Höidén-Guthenberg I, Bönisch H, Guneriusson E, Frejd FY, et al. An engineered affibody molecule with pH-dependent binding to FcRn mediates extended circulatory half-life of a fusion protein. Proc Natl Acad Sci USA. 2014;111:17110–5.

Publisher's Note